

## TABLE OF CONTENTS

### COMMUNICATIONS

**Thermal conversion of gels to  $\text{YBa}_2\text{Cu}_3\text{O}_x$ ,  $\text{Bi}_2\text{Sr}_2\text{CaCu}_2\text{O}_x$ , and  $(\text{Bi,Pb})_2\text{Sr}_2\text{Ca}_2\text{Cu}_3\text{O}_x$  and their decarbonization by low-temperature treatment with nitric acid**

A. Deptula, T. Olczak, W. Lada, K.C. Goretta, A. Di Bartolomeo, A. Brignocchi

**Crack path in an amorphous material in the quasi static limit**

R. Thomson

### ARTICLES

**Solid-state processing and phase development of bulk  $(\text{MgO})_w/\text{BPSCCO}$  high-temperature superconducting composite**

Y.S. Yuan, M.S. Wong, S.S. Wang

**Whisker/matrix interface and microstructure of MgO-whisker reinforced  $(\text{Bi,Pb})_2\text{Sr}_2\text{Ca}_2\text{Cu}_3\text{O}_x$  high-temperature superconducting composite**

Y.S. Yuan, M.S. Wong, S.S. Wang

**A two-powder process for Bi-2223 precursors**

T.G. Holesinger, K.V. Salazar, D.S. Phillips, B.L. Sargent, J.K. Bremser, J.F. Bingert, J.O. Willis, D.E. Peterson

**Preparation and properties of spray dried precursor powder for melt processed bulk YBCO ceramics**

W. Lo, D.A. Cardwell, S-L. Dung, R.G. Barter

**Lattice distortion of thick epitaxial layers**

K. Bickmann, J. Hauck

**A study of enhanced phosphorus activity in n-type  $\text{Si}_{80}\text{Ge}_{20}$  as a function of the doping process**

S.H. Han, B.A. Cook

**Latest developments for microstructural and chemical characterization of diffusion bonding in superplastic 8090 Al-Li alloys**

A. Ureña, J.M. Gómez de Salazar, J.J. Martín, J. Quiñones

**Full-density nanocrystalline Fe-29Al-2Cr intermetallic consolidated from mechanically-milled powders**

L. He, E. Ma

**Relationships between thermomechanical treatments, microstructure and tensile properties of a near beta titanium alloy:  $\beta\text{CEZ}$ : Part I.**

**Relationships between thermomechanical treatments and microstructure**

L. Mora, C. Quesne, C. Haut, C. Servant, R. Penelle

**Relationships between thermomechanical treatments, microstructure and tensile properties of a near beta titanium alloy:  $\beta\text{CEZ}$ : Part II.**

**Relationships between thermomechanical treatments and tensile properties**

L. Mora, C. Quesne, R. Penelle

**Processing of calcium metaphosphate based glass-ceramic coatings on alumina**

K.J. Vaidya, L.F. Francis

**Development of novel microstructures in zirconia-toughened alumina using rapid solidification and shock compaction**

J. Freim, J. McKittrick, W. J. Nellis, J.D. Katz

**The microstructure and creep deformation of hot-pressed  $\text{Si}_3\text{N}_4$  with different amounts of sintering additives**

S-Y. Yoon, T. Akatsu, E. Yasuda

**The infrared dielectric properties of  $\eta\text{-Al}_2\text{O}_3$**

C. Pecharromás, T. González-Carreño, J.E. Iglesias

**Sol-gel synthesis of phosphate ceramic composites-I**

B.I. Lee, W.D. Samuels, L-Q. Wang, G.J. Exarhos

**Amorphous ceramics as the particulate phase in electrorheological materials systems**

D.R. Gamota, A.W. Schubring, B.L. Mueller, F.E. Filisko

**Continuous precipitation of monodispersed colloidal particles. II.  $\text{SiO}_2$ ,  $\text{Al}(\text{OH})_3$  and  $\text{BaTiO}_3$**

Y-S. Her, S-H. Lee, E. Matijević

**Combustion syntheses for  $\text{BaTi}_4\text{O}_9$  and  $\text{Pb}_x\text{Ba}_{1-x}\text{Ti}_4\text{O}_9$**

Z. Zhong, P.K. Gallagher

**Growth of  $(\text{Ba}, \text{Sr})\text{TiO}_3$  thin films by the hydrothermal-electrochemical method and effect of oxygen evolution on their microstructure**

K. Kajiyoshi, M. Yoshimura, Y. Hamaji, K. Tomono, T. Kasanami

**Measurement and interpretation of strain relaxation in passivated Al-0.5% Cu lines**

P.R. Besser, T.N. Marieb, J. Lee, P.A. Flinn, J.C. Bravman

**Electrochemical synthesis of barium titanate thin films**

R.R. Bacsa, G. Rutsch, J.P. Dougherty

**Electrical properties of sol-gel derived films containing composites of glass-ceramics and nanocrystalline silver**

T.K. Kundu, D. Chakravorty

**Damage-resistant alumina-based layer composites**

L. An, H.M. Chan, N.P. Padture, B.R. Lawn

**Structural and microstructural features of pyrite FeS<sub>2-x</sub> thin films obtained by thermal sulfuration of iron**

C. de las Heras, J.L. Martín de Vidales, I.J. Ferrer, C. Sánchez

**Comparison of diamond-like carbon film deposition by electron cyclotron resonance with benzene and methane**

P.S. Andry, P.W. Pastel, W.J. Varhue

**Chromium implantation in silica glass**

E. Cattaruzza, R. Bertonecello, F. Trivillin, P. Mazzoldi, G. Battaglin, L. Mirengi, P. Rotolo

**Optical properties of polymeric thin films grown by chemical vapor deposition**

J.F. Gaynor, S.B. Desu

**REVIEW****Principles of the development of a silica dielectric for microelectronics packaging**

T.K. Gupta, J-H. Jean

**ABSTRACTS****COMMUNICATIONS****Thermal conversion of gels to YBa<sub>2</sub>Cu<sub>3</sub>O<sub>x</sub>, Bi<sub>2</sub>Sr<sub>2</sub>CaCu<sub>2</sub>O<sub>x</sub>, and (Bi,Pb)<sub>2</sub>Sr<sub>2</sub>Ca<sub>2</sub>Cu<sub>3</sub>O<sub>x</sub> and their decarbonization by low-temperature treatment with nitric acid**

A. Deptula\*, T. Olczak\*, W. Lada\*, K.C. Goretta\*, A. Di Bartolomeo#, A. Brignocchi#

(\*Institute of Nuclear Chemistry and Technology, \*Argonne National Laboratory, #ENEA)

Thermal conversion of acetate-derived gels to YBa<sub>2</sub>Cu<sub>3</sub>O<sub>x</sub> (Y-123), Bi<sub>2</sub>Sr<sub>2</sub>CaCu<sub>2</sub>O<sub>x</sub> (Bi-2212), and (Bi,Pb)<sub>2</sub>Sr<sub>2</sub>Ca<sub>2</sub>Cu<sub>3</sub>O<sub>x</sub> (Bi-2223) has been studied by thermal analysis, x-ray diffraction, and infrared spectroscopy. Carbonates formed above 200°C during thermal treatment of all gels. Decomposition of the carbonates proved to be more difficult for Y-123 than for Bi-2212 or Bi-2223. However, all of the gels that were heated contained significant amounts of carbon after calcination. Complete decarbonization of materials was attained by treating the intermediate phases (e.g., those formed after calcination at 600°C) with nitric acid and then subjecting them to a final thermal treatment. Removal of carbonates from the intermediate phases strongly accelerated formation of the superconducting compounds.

Order No.: JA601-001

© 1995 MRS

**Crack path in an amorphous material in the quasi static limit**

R. Thomson

(National Institute of Standards and Technology)

Crack path stability is discussed, and it is shown that the standard continuum mechanics *G*-force on a crack is the correct driving force for a crack. In a glass, where all cleavage planes are possible, this criterion also implies a path where the local Mode II on the crack is nullified.

Order No.: JA601-002

© 1995 MRS

**ARTICLES****Solid-state processing and phase development of bulk (MgO)<sub>w</sub>/BPSCCO high-temperature superconducting composite**

Y.S. Yuan, M.S. Wong, S.S. Wang

(University of Houston)

The inherently weak mechanical properties associated with monolithic high temperature superconductors (HTS) can be improved by introducing properly selected strong ceramic whiskers into the HTS materials. In this research, processing and superconducting properties of monolithic Pb-doped Bi-2223 (BPSCCO) and MgO whisker-reinforced BPSCCO HTS composite materials have been systematically studied. A solid-state processing method is successfully developed to fabricate the (MgO)<sub>w</sub>/BPSCCO composite. The HTS composite contains a dense and

highly pure BPSCCO matrix phase with a preferred grain orientation, which is reinforced by MgO whiskers randomly oriented in the plane perpendicular to the hot-pressing direction. The HTS composite material is shown to exhibit excellent superconducting properties. For example, a transport J<sub>c</sub> measured at 77 K in a zero field has been obtained to exceed 5,000 A/cm<sup>2</sup> in a (MgO)<sub>w</sub>/BPSCCO composite with 10% MgO whiskers by volume. Relationships among solid-state processing variables, HTS phase development, and superconducting properties of the monolithic BPSCCO and the HTS composite are established in the paper.

Order No.: JA601-003

© 1995 MRS

**Whisker/matrix interface and microstructure of MgO-whisker reinforced (Bi,Pb)<sub>2</sub>Sr<sub>2</sub>Ca<sub>2</sub>Cu<sub>3</sub>O<sub>x</sub> high-temperature superconducting composite**

Y.S. Yuan, M.S. Wong, S.S. Wang

(University of Houston)

In this paper, a comprehensive study of the microstructure and the whisker/matrix interface of a (MgO)<sub>w</sub>/BPSCCO high-temperature superconducting composite is reported. The bulk MgO-whisker reinforced HTS BPSCCO (2223) composite was fabricated, using a recently developed solid-state processing method. The (MgO)<sub>w</sub>/BPSCCO composite has been demonstrated to possess excellent combined superconducting and mechanical properties. The favorable microstructure of the HTS BPSCCO (2223) matrix and the (MgO)<sub>w</sub>/BPSCCO interfacial properties are recognized to be the critical material parameters governing electric and mechanical performance of the HTS composite. Effects of detailed microstructure variables on superconducting properties of the composite are addressed, including the aspect ratio and the orientation of MgO whiskers, structure and texturing of the BPSCCO matrix phase, and the (MgO)<sub>w</sub>/BPSCCO interfacial microchemistry. The results obtained reveal unique characteristics of the reinforcing MgO whiskers dispersion, distribution and orientation in the HTS composites. The evolution of the microstructure and texture of the matrix BPSCCO grains have also been studied in the process of repeated hot pressing and annealing heat treatment. The thermodynamic compatibility and microchemistry in the MgO whisker and BPSCCO interface are also examined.

Order No.: JA601-004

© 1995 MRS

**A two-powder process for Bi-2223 precursors**

T.G. Holesinger, K.V. Salazar, D.S. Phillips, B.L. Sargent, J.K. Bremser, J.F. Bingert, J.O. Willis, D.E. Peterson

(Los Alamos National Laboratory)

A two-powder process is described for the production of uniform, fine-grained Bi<sub>2</sub>Sr<sub>2</sub>Ca<sub>2</sub>Cu<sub>3</sub>O<sub>y</sub> (Bi-2223) powders. One powder is the Bi<sub>2-1-x</sub>Pb<sub>x</sub>Sr<sub>1.9-y</sub>Ca<sub>y</sub>O<sub>z</sub> (2:2 Cu-free) phase. The other is a multi-phase powder of approximate overall composition SrCaCu<sub>3</sub>O<sub>y</sub>. The 2:2 Cu-free is one of the first Bi-containing phases to form from a nominal Bi-2223

mixture of oxides and carbonates. The powders have very similar particle morphologies and the mixing volumes are closely matched. Critical current densities up to 26,900 A/cm<sup>2</sup> in self field at 75 K were obtained in tapes.

Order No.: JA601-005

© 1995 MRS

#### Preparation and properties of spray dried precursor powder for melt processed bulk YBCO ceramics

W. Lo, D.A. Cardwell, S-L. Dung, R.G. Barter  
(University of Cambridge)

YBa<sub>2</sub>Cu<sub>3</sub>O<sub>7-δ</sub> precursor powder suitable for the fabrication of melt processed ceramic has been prepared by spray drying and subsequent calcination. The dehydration and decomposition processes in the nitrate-based spray dried powder and the formation processes of the YBa<sub>2</sub>Cu<sub>3</sub>O<sub>7-δ</sub> and Y<sub>2</sub>BaCuO<sub>5</sub> phases have been studied in detail using thermal analysis and powder x-ray diffractometry. The morphology, microstructure and size distribution of the particles in the calcined powder have been investigated using high resolution scanning electron microscopy and particle size analysis and found to contain a significant proportion of submicron sized particles of Y<sub>2</sub>BaCuO<sub>5</sub>. Melt processed samples prepared using the spray dried powder have been observed to exhibit a significantly finer distribution of the 211 phase than is typically obtained in similar specimens prepared via a mixed oxide route. This provides direct evidence of the suitability of spray dried precursor powder for the fabrication of large grain, high J<sub>c</sub> melt processed YBCO ceramics.

Order No.: JA601-006

© 1995 MRS

#### Lattice distortion of thick epitaxial layers

K. Bickmann, J. Hauck  
(Institut für Festkörperforschung)

Precise x-ray diffraction measurements between room temperature and ~400°C (Bond method) exhibit some details in the variations of strain in ~1 μm thick epitaxial layers of GaAs, InP, CdTe, EuS or SrS on Si or GaAs substrates. The lattice parameters of the cubic layers, which are deposited at high temperatures, deviate from the lattice parameters, a<sub>0</sub>, of small unconstrained single crystals by  $\Delta a/a_0 = \epsilon^0 \lesssim 10^{-3}$ . The layers adhere to the substrates below T<sub>c</sub> and adopt different strains,  $\epsilon''$  and  $\epsilon^\perp$ , parallel and perpendicular to the substrate. Frequently the T<sub>c</sub> and  $\epsilon^0$  values vary on annealing at 160–400°C. The ratio  $E = -(\epsilon^\perp - \epsilon^0)/(\epsilon'' - \epsilon^0)$  remains constant for each sample. The change of the relative volume  $\Delta V/V_0 = \epsilon''(2-E) + \epsilon^0(1+E)$  at the variation of  $\epsilon''$  and  $\epsilon^0$  can give rise to corrugations, blisters or microcracks in the epitaxial layers. Stable epitaxial layers with constant  $\epsilon^0$  and T<sub>c</sub> values can be obtained by deposition on buffer layers or stepped substrates.

Order No.: JA601-007

© 1995 MRS

#### A study of enhanced phosphorus activity in n-type Si<sub>80</sub>Ge<sub>20</sub> as a function of the doping process

S.H. Han, B.A. Cook  
(Ames Laboratory)

The electrical activity of phosphorus in Si<sub>80</sub>Ge<sub>20</sub> alloys prepared by two nonconventional doping processes has been investigated over the temperature range 25–1250°C. Both solid state (mechanical alloying) and gaseous phase doping processes were found to extend the electrical activity of phosphorus in Si<sub>80</sub>Ge<sub>20</sub> alloys beyond the reported maximum equilibrium value (2.1×10<sup>20</sup>/cm<sup>3</sup>) to 2.5–2.9×10<sup>20</sup>/cm<sup>3</sup> within the temperature range 900 to 1200°C. It is likely that this extended electrical activity of phosphorus is associated with a high density of defects. The enhanced electrical activity of phosphorus enabled Si<sub>80</sub>Ge<sub>20</sub> alloys to have 300 to 1000°C integrated average electrical power factors in the range 30.1–35.7 μW/cm<sup>2</sup>·°C<sup>2</sup>.

Order No.: JA601-008

© 1995 MRS

#### Latest developments for microstructural and chemical characterization of diffusion bonding in superplastic 8090 Al-Li alloys

A. Ureña, J.M. Gómez de Salazar, J.J. Martín, J. Quiñones  
(Universidad Complutense de Madrid)

This paper describes a new application of two complementary surface characterization techniques to study solid state bonding in an Al-Li alloy. Through the two mentioned techniques, atomic force microscopy (AFM) and secondary ion mass spectrometry (SIMS), important findings about what takes place in the bond interface have been determined. These findings include both the formation of discontinuous mixed oxides and the evolution of Li through the bond line and into the adjacent diffusion affected zones. Homogenization of Li and Cu alloy elements has been detected even in those cases where a metallic interlayer was used to favor the union.

Order No.: JA601-009

© 1995 MRS

#### Full-density nanocrystalline Fe-29Al-2Cr intermetallic consolidated from mechanically-milled powders

L. He, E. Ma  
(Louisiana State University)

Fe-29Al-2Cr powders with nanoscale grain sizes were produced by mechanical milling of pre-alloyed intermetallic powders. A consolidation procedure employing high-pressure, low strain rate hot forging (sinter-forging) has been developed to consolidate the powders into full-density compacts. The relative density and average grain size of the compact have been studied as a function of consolidation temperature at constant pressure. Fully-dense compacts (>99.5% theoretical density) were produced at a relatively low temperature of 545°C with a pressure of 1.25 GPa. Transmission electron microscopy and x-ray diffraction analysis indicate that the average grain size has been maintained to the order of 30 nm in samples consolidated under these conditions. By using protective Ar atmosphere during mechanical milling and consolidation, contamination of oxygen and carbon in consolidated samples has been controlled to below a small fraction of an atomic percent. Microhardness tests of nanocrystalline Fe-29Al-2Cr samples indicate a significant strengthening effect due to grain size refinement and a monotonic hardness increase with decreasing residual porosity. Our work demonstrates the feasibility of using mechanically-milled powders as a source of nanocrystalline materials for the production of fully-dense, low-impurity, nanocrystalline bulk samples needed for reliable mechanical property measurements and practical applications.

Order No.: JA601-010

© 1995 MRS

#### Relationships between thermomechanical treatments, microstructure and tensile properties of a near beta titanium alloy: βCEZ: Part I.

Relationships between thermomechanical treatments and microstructure  
L. Mora, C. Quesne, C. Haut, C. Servant, R. Penelle  
(Université de Paris-Sud)

The high strength medium temperature and β metastable titanium alloy, βCEZ, is designed for use in the compressor of a jet engine. The purpose of this research was to investigate how the thermomechanical treatments (forging or solutioning conditions and quenching) influence the microstructure. A series of various heat treating steps were conducted in order to quantify the relationship between thermomechanical parameters and microstructural factors. The detailed characterization of microstructure was based on SEM observations of primary alpha platelets with the aid of an Image Analysis system. A pronounced influence of thermomechanical treatments on microstructure was found. Several parameters characterizing the microstructure of alpha platelets such as the area fraction, the length, the width, the perimeter, the surface, the density and the aspect ratio, have been found to depend on the solutioning conditions. Furthermore, with the exception of the area fraction, these different microstructural parameters were found to also be governed by the forging conditions.

Order No.: JA601-011

© 1995 MRS

**Relationships between thermomechanical treatments, microstructure and tensile properties of a near beta titanium alloy:  $\beta$ CEZ: Part II.**

**Relationships between thermomechanical treatments and tensile properties**

L. Mora, C. Quesne, R. Penelle  
(Université de Paris-Sud)

The tensile properties of the beta-CEZ titanium alloy (Ti Al, 2Sn, 4Zr, 4Mo, 2Cr, 1Fe weight %) have been investigated at intermediate temperature as a function of the thermomechanical treatments. The strength and ductility have been correlated with the microstructural changes caused by the various heat treatments. It is found that the highest yield strength is associated with a structure containing a small area fraction, a small size and a high density of primary alpha platelets ( $\alpha_p$ ). Moreover, the size of the secondary alpha phase ( $\alpha_s$ ) has been found to affect the yield strength. It is concluded that the ductility is enhanced by a high area fraction of  $\alpha_p$  platelets and is also sensitive to the density and the morphological orientation of the  $\alpha_p$  platelets. The interfaces between the  $\alpha_p$  and  $\beta$  phases play a dominant role in beta-CEZ tensile behavior, and transgranular fracture is the main failure feature of this alloy.

Order No.: JA601-012 © 1995 MRS

**Processing of calcium metaphosphate based glass-ceramic coatings on alumina**

K.J. Vaidya, L.F. Francis  
(University of Minnesota)

Dense, crystalline, glass-ceramic coatings containing calcium metaphosphate and aluminum phosphate were prepared on aluminum oxide substrates by a three step method. The processing involved glass (40 mol% CaO, 10% Al<sub>2</sub>O<sub>3</sub>, 50% P<sub>2</sub>O<sub>5</sub>) formation, deposition of a glass particle coating and heat treatment to sinter the glass and crystallize the phosphates. Sintering and microstructure evolution were influenced by wet coating thickness, heat treatment temperature, time, and heating rate. Heat treatment for 1 hour at 725°C using a 50°C/min heating rate was found to give a dense, crack-free coating. The resultant coating microstructure has spherulitic morphology (0.3  $\mu$ m size) with aluminum phosphate in the center of the spherulite. The hardness of the fully crystallized glass-ceramic coating was ~5.2 GPa.

Order No.: JA601-013 © 1995 MRS

**Development of novel microstructures in zirconia-toughened alumina using rapid solidification and shock compaction**

J. Freim\*, J. McKittrick\*, W. J. Nellis\*, J.D. Katz#  
(\*University of California at San Diego, #Lawrence Livermore National Laboratory, #Los Alamos National Laboratory)

A rapidly solidified alumina-zirconia eutectic material containing nanocrystalline t-ZrO<sub>2</sub> has been synthesized. When heated the microstructure contained a mixture of t-ZrO<sub>2</sub> and m-ZrO<sub>2</sub>, each of which can facilitate toughening of the composite. Dynamic shock compaction was used to accelerate densification of the material, producing crack free specimens with high green densities. After sintering to densities measuring ~95% of theoretical, the shock compacted specimens fabricated with unstabilized alumina-zirconia were extensively microcracked due to an overabundance of the m-ZrO<sub>2</sub> phase. Experiments employing Y<sub>2</sub>O<sub>3</sub> as a chemical stabilizer have shown that the extent of the phase transformation can be controlled, and the microstructure which developed in the stabilized material contained an acceptable level of the microcrack generating m-ZrO<sub>2</sub> phase.

Order No.: JA601-014 © 1995 MRS

**The microstructure and creep deformation of hot-pressed Si<sub>3</sub>N<sub>4</sub> with different amounts of sintering additives**

S.-Y. Yoon, T. Akatsu, E. Yasuda  
(Tokyo Institute of Technology)

Compressive creep deformation of hot-pressed silicon nitride with different amounts of grain boundary glassy phase was investigated at

1300-1400°C under 30-100 MPa. The stress exponent of the creep rate was determined to be nearly unity. The apparent activation energy of silicon nitride with larger amount of glassy phase was measured to be about 700 kJ/mole, and that with smaller amount of glassy phase was found to be 400 kJ/mole. In addition, the microstructural observation found that no cavity appeared and grain boundary glass was recrystallized during creep test. Thus, the rate-limiting steps in solution/precipitation creep mechanism change from the solution-precipitation of Si<sub>3</sub>N<sub>4</sub> grains to the diffusion through the grain boundary while increasing the amount of glassy phase.

Order No.: JA601-015 © 1995 MRS

**The infrared dielectric properties of  $\eta$ -Al<sub>2</sub>O<sub>3</sub>**

C. Pecharrómán, T. González-Carreño, J.E. Iglesias  
(Consejo Superior de Investigaciones Científicas)

The infrared complex permittivity function of pseudo-cubic, disordered, spinel type variety of alumina,  $\eta$ -Al<sub>2</sub>O<sub>3</sub>, obtained by spray pyrolysis, has been determined from its IR reflectance spectra, measured at near to normal incidence on pressed powder pellets. The optical constants obtained therefrom have been verified by using them in the simulation of the corresponding absorption spectra for KBr-diluted pellets of this material, and these are in excellent agreement with the experimental spectra. All calculations are based on a procedure for the estimation of the effective dielectric function of a mixture incorporating percolation features, which has been recently developed by the authors.

Order No.: JA601-016 © 1995 MRS

**Sol-gel synthesis of phosphate ceramic composites-I**

B.I. Lee\*, W.D. Samuels\*, L.-Q. Wang\*, G.J. Exarhos\*  
(\*Clemson University, \*Battelle Pacific Northwest Laboratory)

Monolithic gels of phosphate ceramics were synthesized using PO(OH)<sub>3-x</sub>(OR)<sub>x</sub> and alkoxides of silicon and titanium. The PO(OH)<sub>3-x</sub>(OR)<sub>x</sub> species were synthesized from the reaction of P<sub>2</sub>O<sub>5</sub> and ethanol or n-butanol and the products consisted of approximately equal molar amounts of mono- and dialkyl phosphate. The phosphate gels containing titanium lost less phosphorus than the gels of silicon/phosphorus upon firing of the gels in air. At phosphorus contents above 60 mole %, the gels were completely crystallized upon firing at temperatures above 700°C. The gels containing zinc and alkali metals remained amorphous after firing at 850°C. Solid state nuclear magnetic resonance spectroscopy showed that all of the silicon is hexa-coordinated in the phosphate gels containing silicon and titanium upon firing at temperatures above 520°C.

Order No.: JA601-017 © 1995 MRS

**Amorphous ceramics as the particulate phase in electrorheological materials systems**

D.R. Gamota\*, A.W. Schubring†, B.L. Mueller#, F.E. Filisko§  
(\*Motorola, †Delco Electronics Corporation, #Henkel Corporation, §The University of Michigan)

Several electrorheological (ER) materials systems composed of amorphous ceramic powders dispersed in light paraffin oil were developed to determine if relationships between ER activities, dielectric properties, compositions, porosities, and oxide species could be identified. The results of the studies suggested that trends between ER activity, dielectric phenomena, and alkali metal species existed. The aluminosilicate powders developed with various alkali metals showed that the ER activity increased as the activation energy decreased. The sodium aluminosilicate appeared to have the greatest ER activity and the lowest activation energy, while the cesium aluminosilicate displayed the weakest ER response, but had the highest activation energy. The thermodielectric responses of the different oxide materials systems developed with sodium showed that the mechanisms contributing to the dielectric dispersions had similar activation energies; however, the magnitudes of the recorded ER activities varied and thus a direct correlation was not apparent. In

addition, studies conducted with ER materials composed of sodium aluminosilicate powders of varying porosities showed that ER activities increased with increasing porosity. Furthermore, the analysis of the results of the thermodielectric and rheological studies of the different amorphous materials ER systems suggested that these materials may have an optimum stimulus frequency/temperature for ER activity.

Order No.: JA601-018

© 1995 MRS

#### Continuous precipitation of monodispersed colloidal particles.

##### II. $\text{SiO}_2$ , $\text{Al}(\text{OH})_3$ and $\text{BaTiO}_3$

Y-S. Her, S-H. Lee, E. Matijević  
(Clarkson University)

Colloidal spherical particles of  $\text{SiO}_2$ ,  $\text{Al}(\text{OH})_3$ , and  $\text{BaTiO}_3$  of narrow size distributions were produced in a continuous static mixer tubular reactor system. Several experimental parameters, including the flow rate, reaction temperature and time, reactant concentrations, and the dimensions of the reactor, were varied in order to establish the optimum conditions required for each material. The results were compared with those obtained in batch systems. Monodispersed colloids can be generated at a rate as high as 50 pounds per day using the described laboratory scale continuous reactor.

Order No.: JA601-019

© 1995 MRS

#### Combustion syntheses for $\text{BaTi}_4\text{O}_9$ and $\text{Pb}_x\text{Ba}_{1-x}\text{Ti}_4\text{O}_9$

Z. Zhong, P.K. Gallagher  
(The Ohio State University)

$\text{BaTi}_4\text{O}_9$  and  $\text{Pb}_x\text{Ba}_{1-x}\text{Ti}_4\text{O}_9$ , where  $x$  is 0.1, 0.2, 0.3, 0.4 or 0.5, have been prepared by a combustion synthesis process. The process starts with spray drying aqueous solutions of  $\text{Pb}(\text{NO}_3)_2$ ,  $\text{Ba}(\text{NO}_3)_2$ ,  $\text{TiO}(\text{NO}_3)_2$  and  $\beta$ -alanine with appropriate ratios. Combustion reactions occur when heating the spray dried products to  $300^\circ\text{C}$ , which convert them to  $\text{BaTi}_4\text{O}_9$  and  $\text{Pb}_x\text{Ba}_{1-x}\text{Ti}_4\text{O}_9$  directly.  $\text{Pb}_x\text{Ba}_{1-x}\text{Ti}_4\text{O}_9$  ( $x \geq 0.1$ ) are low temperature, metastable phases and have not been reported before.  $\text{Pb}_{0.5}\text{Ba}_{0.5}\text{Ti}_4\text{O}_9$  is unstable above  $800^\circ\text{C}$  and cannot be sintered. All  $\text{Pb}_x\text{Ba}_{1-x}\text{Ti}_4\text{O}_9$  compositions will decompose by  $1300^\circ\text{C}$ , the temperature for solid state synthesis of  $\text{BaTi}_4\text{O}_9$ . Single-phase  $\text{Pb}_x\text{Ba}_{1-x}\text{Ti}_4\text{O}_9$ , ( $x=0.1, 0.2, 0.3, 0.4$ ), however, have been sintered at relatively lower temperatures.

Order No.: JA601-020

© 1995 MRS

#### Growth of (Ba, Sr)TiO<sub>3</sub> thin films by the hydrothermal-electrochemical method and effect of oxygen evolution on their microstructure

K. Kajiyoshi\*, M. Yoshimura\*, Y. Hamaji\*, K. Tomono\*, T. Kasanami\*  
(\*Murata Manufacturing Co., Ltd., \*Tokyo Institute of Technology)

Thin films in the system  $\text{BaTiO}_3$ - $\text{SrTiO}_3$  have been grown on Ti electrodes with control of the Ba/Sr composition in aqueous solutions of  $(\text{Ba, Sr})(\text{OH})_2$  by the hydrothermal-electrochemical method. Barium contents of the solid-solution films were always lower than those of the synthesis solutions used. The  $\text{BaTiO}_3$  and the (Ba, Sr)TiO<sub>3</sub> solid-solution films included "crater-shape" defects that resulted from the breakaway of the growing film, whereas no such defects were observed in the  $\text{SrTiO}_3$  film. This dependence of the defect generation on the film composition was interpreted to be caused by differences of anodically evolved oxygen gas pressure in "short circuiting paths" that exist characteristically in the films grown by this method.

Order No.: JA601-021

© 1995 MRS

#### Measurement and interpretation of strain relaxation in passivated Al 0.5% Cu lines

P.R. Besser\*, T.N. Marieb\*, J. Lee\*, P.A. Flinn#, J.C. Bravman#  
(\*Advanced Micro Devices, Inc., \*Intel Corporation, #Stanford University)

X-ray diffraction has been used to measure the strain relaxation in passivated Al-0.5%Cu lines at  $200^\circ\text{C}$  after cooling directly from an anneal at the passivation deposition temperature of  $380^\circ\text{C}$ . Fits to the measured X, Y and Z components of strain are summed to obtain the hydrostatic component, which exhibits a decay over time. Three mechanisms are

considered to explain the decay of the hydrostatic strain in the metal line: Cu precipitation from the solid solution, the presence and growth of voids in the lines, and time-dependent deformation of the passivation. Calculations of the effect of Cu precipitation from the solid solution demonstrate that it plays an insignificant role in the relaxation. A high-voltage scanning electron microscope is used to image the presence and growth of voids through the passivation. The time scale of the growth of stress-induced voids is not the same as the hydrostatic relaxation, indicating that voiding is not solely responsible for the observed relaxation. The relaxation of the line is modeled using a time-dependent finite element model allowing elastic compliance of the passivation. The magnitude of the calculated relaxation agrees with the measurements. It is suggested that a combination of voiding and passivation compliance is responsible for the measured hydrostatic strain relaxation in the metal line.

Order No.: JA601-022

© 1995 MRS

#### Electrochemical synthesis of barium titanate thin films

R.R. Bacsa, G. Rutsch, J.P. Dougherty  
(The Pennsylvania State University)

Polycrystalline films of barium titanate ( $\text{BaTiO}_3$ ) have been synthesized on titanium (Ti) substrates by the galvanostatic anodization of Ti in a solution of 0.4 M  $\text{Ba}(\text{OH})_2$ . Crystalline films are formed at temperatures under  $100^\circ\text{C}$  within 10 min. at a current density of  $25 \text{ mA/cm}^2$  at atmospheric pressure. Crystallinity of the films is found to increase with both current density and time of reaction. At  $90^\circ\text{C}$ , a film of  $1 \mu\text{m}$  thickness is formed after 10 minutes; grain sizes up to  $0.5 \mu\text{m}$  are obtained. Microstructure of the films is found to be critically dependent on the pretreatment of the titanium anode. Capacitance measurements on the film yield a dielectric constant of 200 with a minimum  $\tan \delta$  of 0.09 at 10 kHz. On the basis of the voltage-time curves, it is interpreted that an amorphous intermediate is formed which crystallizes to form perovskite  $\text{BaTiO}_3$ .

Order No.: JA601-023

© 1995 MRS

#### Electrical properties of sol-gel derived films containing composites of glass-ceramics and nanocrystalline silver

T.K. Kundu, D. Chakravorty  
(Indian Association for the Cultivation of Science)

Sol-gel derived films containing  $\text{BaTiO}_3$  crystallites have been grown on suitable substrates using a precursor composition in the system  $\text{Li}_2\text{O-BaO-TiO}_2$ . Silver particles of diameters in the range 4.9 to 16.2 nm have been synthesized within these films by ion exchange and reduction technique. Electrical resistivities are found to vary from  $\sim 10^2$  to  $10^5 \text{ ohm-cm}$  depending on the silver particle diameter. A low activation energy, approximately a few milli electron volts, is found to characterize the electrical property of most of the samples. A quantum size effect is invoked to explain the results.

Order No.: JA601-024

© 1995 MRS

#### Damage-resistant alumina-based layer composites

L. An\*, H.M. Chan\*, N.P. Padture\*, B.R. Lawn#  
(\*Lehigh University, #National Institute of Standards and Technology)

A new philosophy for tailoring layer composites for damage resistance is developed, specifically for alumina-based ceramics. The underlying key to the approach is microstructural control in the adjacent layers, alternating a traditional *homogeneous* fine-grain alumina (layer **A**) for hardness and wear resistance with a *heterogeneous* alumina:calcium-hexaluminate composite (layer **C**) for toughness and crack dispersion, with strong bonding between the interlayers. Two trilayer sequences, **ACA** and **CAC**, are investigated. Hertzian indentation tests are used to demonstrate the capacity of the trilayers to absorb damage. In the constituent materials, the indentation responses are fundamentally different: ideally brittle in material **A**, with classical cone cracking outside the contact; quasi-plastic in material **C**, with distributed microdamage beneath the contact. In the **ACA** laminates, shallow cone cracks form in the outer **A** layer, together with a partial microdamage zone in the inner **C** layer. A

feature of the cone cracking is that it is substantially shallower than in the bulk **A** specimens and does not penetrate to the underlayer, even when the applied load is increased. This indicates that the subsurface micro-damage absorbs significant energy from the applied loads, and thereby "shields" the surface cone crack. Comparative tests on **CAC** laminates show a constrained microdamage zone in the outer **C** layer, with no cone crack, again indicating some kind of shielding. Importantly, interlayer delamination plays no role in either layer configuration; the mechanism of damage control is by crack *suppression* rather than by *deflection*. Implications for the design of synergistic microstructures for damage-resistant laminates are considered.

Order No.: JA601-025

© 1995 MRS

#### Structural and microstructural features of pyrite $\text{FeS}_{2-x}$ thin films obtained by thermal sulfuration of iron

C. de las Heras, J.L. Martín de Vidales, I.J. Ferrer, C. Sánchez  
(Universidad Autónoma de Madrid)

Structural and microstructural properties of synthetic thin films of pyrite, ( $\text{FeS}_{2-x}$ ), prepared by thermal sulfuration of iron layers, were investigated from Rietveld refinements of x-ray diffraction data, collected by step/scan mode. From this refinement lattice constant, **a**, and sulfur position parameter, **u**, nearest neighbor Fe-S and S-S bond distances and tetrahedral and octahedral bond angles have been determined. Moreover, sulfur deficit in the samples, surface and volume-weighted crystallite size and microstrains were also obtained. From these data, the influence of temperature and time of sulfuration and sulfur pressure on their structural and microstructural properties has been established. Stoichiometric pyrite thin films are obtained by sulfurating the iron films at low temperatures ( $T_S \sim 600\text{--}700\text{ K}$ ) during short times ( $t_S \sim 0.5\text{--}2\text{ h}$ ). These experimental conditions yield films with the highest **a**, **u**, Fe-S bond distances and microstrains; as well as S/Fe ratios about 2.00, i.e., null sulfur vacancies, the smallest S-S bond distances and crystallite size. Finally, the possible influence of these structural and microstructural characteristics on some physical properties (optical absorption, electrical resistivity, etc.) of the films is discussed.

Order No.: JA601-026

© 1995 MRS

#### Comparison of diamond-like carbon film deposition by electron cyclotron resonance with benzene and methane

P.S. Andry, P.W. Pastel, W.J. Varhue  
(University of Vermont)

A comparative study of the deposition of diamond-like carbon films using methane or benzene in a microwave electron cyclotron resonance plasma enhanced chemical vapor deposition system has been performed. Process variables studied were reactor pressure, applied radio frequency substrate bias and microwave power. The plasma stream was characterized using optical emission spectroscopy and mass spectrometry. Film properties studied included optical energy gap, total hydrogen content, integrated C-H stretch absorption, index of refraction, and Raman spectra. The use of a high C/H ratio reactant such as benzene was found to be advantageous over methane in that higher deposition rates were possible and the resultant films exhibit diamond-like properties without the application of large substrate biases. Another result of this investigation was further confirmation that hard carbon films contain a significant quantity of non-bonded hydrogen.<sup>1</sup>

Order No.: JA601-027

© 1995 MRS

#### Chromium implantation in silica glass

E. Cattaruzza\*, R. Bertoncello\*, F. Trivillin\*, P. Mazzoldi\*, G. Battaglin\*, L. Mirengi#, P. Rotolo#

(\*Interuniversitario Nazionale per la Chimica dei Materiali,

\*Unità dell'Institut Nazionale per la Fisica della Materia,

#Parco Scientifico e Tecnologico Ionico Salentino)

Silica glass was implanted with chromium at the energy of 35 and 160 keV, and at fluences varying from  $1 \times 10^{16}$  to  $11 \times 10^{16}$  ions  $\text{cm}^{-2}$ . In a

set of chromium-implanted samples significant amounts of carbon were detected. Samples were characterized by x-ray photoelectron spectroscopy, x-ray-excited Auger electron spectroscopy, secondary ion mass spectrometry, and Rutherford backscattering spectrometry. Chromium silicide and chromium oxide compounds were observed; the presence of carbon in the implanted layers induces the further formation of chromium carbide species. Thermodynamic considerations applied to the investigated systems supply indications in agreement with the experimental evidences.

Order No.: JA601-028

© 1995 MRS

#### Optical properties of polymeric thin films grown by chemical vapor deposition

J.F. Gaynor, S.B. Desu

(Virginia Polytechnic Institute and State University)

For the first time, the refractive index of polyparaxylylene films, the only polymers grown commercially by chemical vapor deposition (CVD), are reported throughout the visible spectrum. This information is required if optical components such as antireflective coatings or waveguides are to be fabricated with CVD polymers. These properties are compared to a low-index CVD copolymer, poly(parachloroxylylene-co-perfluorooctyl methacrylate), invented in our laboratory. The ellipsometric constants  $\psi$  and  $\Delta$  were measured for wavelengths between 400 nm and 1000 nm using variable angle spectroscopic ellipsometry; many samples of each film were grown to improve statistics. The data was modeled assuming a birefringent Cauchy dispersion; excellent agreement between models and experimental data were obtained. The refractive index ( $\lambda = 632.8\text{ nm}$ ) of the copolymer in the film plane was 1.389, compared to 1.645-1.665 for the homopolymers. PPX, PPX-C and the copolymer showed negative birefringence, while PPX-D showed positive birefringence. The optical properties of PPX showed little thickness dependence for films ranging from 36 nm to 2100 nm thick.

Order No.: JA601-029

© 1995 MRS

## REVIEW

#### Principles of the development of a silica dielectric for microelectronics packaging

T.K. Gupta\*, J-H. Jean\*

(\*Westinghouse Electric Corporation, \*National Tsing Hua University)

Recognizing that *speed*, *size*, *reliability* and *cost* are the principal driving forces for advanced electronic packages, this review article describes the much needed development of a new, phase transformation-free, single-phase silica dielectric with a dielectric constant ( $k$ ) of about 4, the lowest among the inorganic oxides, and a coefficient of thermal expansion (CTE) of about 3 ppm/ $^{\circ}\text{C}$ , similar to that of Si. This dielectric consisting largely of  $\text{SiO}_2$  represents a gain in media speed by about 50% over alumina dielectric, combined with an improvement in reliability of the package by a factor of about 1000. The feature size and system cost can also be drastically reduced by using this dielectric. It is made from a mixture of binary borosilicate glasses that normally exhibit an undesirable characteristic of precipitating cristobalite during sintering that severely weakens the structure. The most important aspect of this article is the design and development of a strategy that prevents the cristobalite growth by incorporating a crystal growth inhibitor in the binary mixture of glasses. Since kinetics, not thermodynamics, are shown to be the key to success of this strategy, the roles of rate-controlling parameters are deliberately emphasized. A working model is delineated to identify compositions that yield a cristobalite-free silica dielectric with values of CTE that match those of Si and GaAs. Critical issues of co-firing between metals and this dielectric are addressed within the context of multilayer packaging fabrication. Finally, a list of measured properties is presented that clearly shows new opportunities for this silica dielectric.

Order No.: JA601-030

© 1995 MRS

Most Comprehensive Database on Ion Beam Analysis Ever Published!

# HANDBOOK OF MODERN ION BEAM MATERIALS ANALYSIS

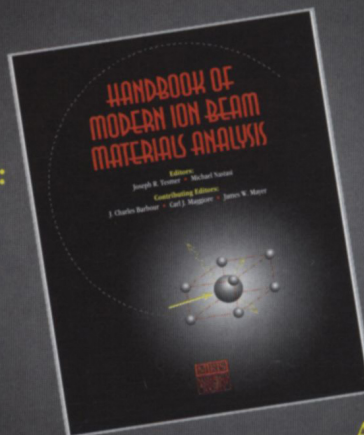
JUST PUBLISHED  
AUGUST 18

## Editors:

Joseph R. Tesmer  
Michael Nastasi

## Contributing Editors:

J. Charles Barbour  
Carl J. Maggiore  
James W. Mayer



The *Handbook of Modern Ion Beam Materials Analysis* is a compilation of updated techniques and data for use in the ion-beam analysis of materials. The information presented is unavailable collectively from any other source, and places a strong emphasis on practical examples of the analysis techniques as they are applied to common problems. The book's 13 chapters cover discussions and examples, while 18 appendices provide extensive compilations of relevant data.

Order the *Handbook of Modern Ion Beam Materials Analysis* today!

1995, Hardbound, 700 Pages  
ISBN: 1-55899-254-5  
Order Code: IBH-CA

**\$160.00 MRS Members**  
**\$200.00 U.S. List**  
**\$230.00 Foreign**

## Chapters

1. Introduction
2. Energy Loss
3. Nuclear Theory
4. Backscattering Spectrometry
5. Elastic Recoil Detection: ERD
6. Nuclear Reaction Analysis: Particle-Particle Reactions
7. Nuclear Reaction Analysis with (Particle,  $\gamma$ ) Reactions
8. Nuclear Reactions for Hydrogen Analysis
9. Charged Particle Activation Analysis
10. Channeling
11. Instrumentation and Laboratory Practice
12. Pitfalls in Ion Beam Analysis
13. Radiological Safety

Written and compiled by over 30 leading authorities in the field of ion beam analysis

Important reference tool for technicians, students and professionals alike

A must for all accelerator labs

Excellent introduction to the lab practices and fundamentals of ion beam analysis

Useful as a teaching text for undergraduate seniors or first-year graduate students

For libraries, the most recent and comprehensive collection of nuclear data for the applications of ion beam materials analysis

## Appendices

1. Elements
2. Physical Constants, Conversions, and Useful Combinations
3. Stopping and Range
4. Scattering and Reaction Kinematics
5. K Factors for RBS
6. Rutherford Cross Sections
7. Non-Rutherford Elastic Backscattering Cross Sections
8. Actual Coulomb Barriers
9. Elastic Recoil Detection Data
10. Deuterium-Induced Nuclear Reaction Parameters
11. Particle-Particle Nuclear Reaction Cross Sections
12. (Particle,  $\gamma$ ) Data
13. Hydrogen Nuclear Reaction Data
14. Activation Analysis Data
15. Channeling Data
16. Thin-Film Materials and Preparation
17. Accelerator Energy Calibration and Stability
18. Radiation Hazards of ( $\alpha, n$ ) Reactions

950188

## Special Savings on Course Adoptions

Order the *Handbook of Modern Ion Beam Materials Analysis* in quantities of five or more (for classroom use) and save up to **20%** on your order!



## Order From:

Materials Research Society  
9800 McKnight Road  
Pittsburgh, PA 15237-6006 USA  
Phone: 412-367-3012; Fax: 412-367-4373